Wall shear rates induced by a single cavitation bubble collapse

[1,2]Fabian Reuter*; [2]Hemant Sagar; [2]Bettar el Moctar; [1]Robert Mettin

[1]*Georg-August-Universität Göttingen, Drittes Physikalisches Institut, Christian Doppler Laboratory for Cavitation and Microerosion, Germany*

[2]*Universität Duisburg-Essen, Institute of Ship Technology, Ocean Engineering and Transport Systems; Germany*

Abstract

When a cavitation bubble collapses in vicinity to a solid surface, high flow velocities are induced. They involve remarkably high but unsteady wall shear rates. Even though they are crucial in ultrasonic surface cleaning or cavitation erosion, and their knowledge is needed for validation of numerical methods, they have not been measured so far due to experimental difficulties. Here, a wall shear rate raster microscope was developed. It bases on an electrochemical principle and involves a model to solve the appropriate convection-diffusion equation. As wall shear rate sensor, a microelectrode was flush-mount into a solid surface. With this method, wall shear rates on micrometer and microsecond scales can be resolved. The wall shear rates produced during the collapse of a single, laser generated bubble (maximum radius about 400 µm) were measured in planes. Via the synchronously performed high speed imaging, the wall shear rates can be clearly related to details and the different stages of the bubble dynamics. This way the respective impacts of the flow phenomena involved on the generation of wall shear stress were evaluated. For example, the jet that accompanies the bubble collapse was resolved in terms of wall shear rates during its impact on the wall and its subsequent spreading in radial direction. The above experimental data are compared with results of numerical simulations of the collapse of a single bubble obtained with a compressible two-phase flow solver that uses barotropic equations of state.

Keywords: bubble collapse, wall shear rates, cavitation

Introduction

Collapsing cavitation bubbles may induce significant mechanical effects on nearby solid surfaces. This is the case for example in ultrasonic cleaning [1][2], cavitation erosion [3][4][5] or cell manipulation [6][7][8]. Most of the mechanical interaction from a cavitation bubble is mediated by the shock wave that is emitted during the bubble collapse [9] and via the intense microflows generated by the bubble dynamics. Because a cavitation bubble can generate its intense microflows directly in the near-wall liquid layer at a solid boundary, the involved flows possess extraordinarily high wall shear rates. However, because the transient bubble dynamics occur are fast and local, the wall shear flows are short-lived and local. Consequently, there are hardly experimental techniques available for their measurement. Thus, the wall shear rates exhibited by cavitation bubbles are largely unknown. Here, we present measurements on the time-resolved wall shear rates produced by a single cavitation bubble. An electrochemical wall shear rate microscope was developed and used to spatially scan the wall shear rates produced by a single laser-induced cavitation bubble. The experimental results are compared to numerical computations performed using a Navier Stokes equations solver implemented in the open source toolbox OpenFOAM [10].

Experimental methods

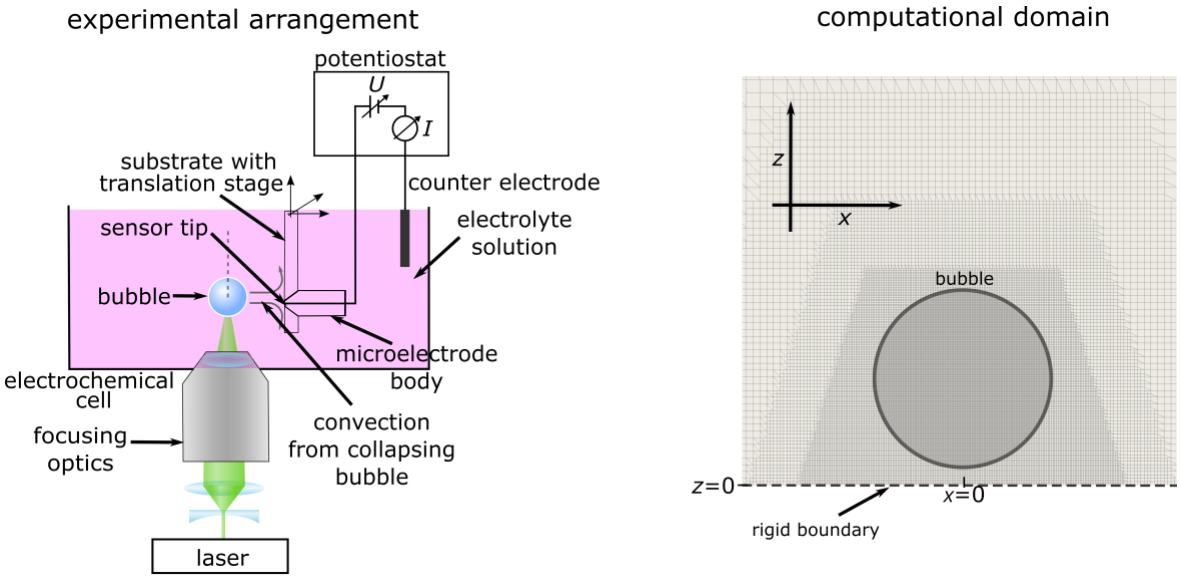

Figure 1 *Left*: Experimental arrangement. *Right*: Discretization of the computational domain with a refinement around the bubble.

To measure the wall shear rates of a single collapsing cavitation bubble, an electrochemical wall shear rate raster microscope was developed, a sketch is given in Figure 1 (left). As sensor, it employs an electrode that is flush-mounted into a solid substrate. The substrate is connected to a two axis precision translation stage (12 nm resolution) to allow for a rastering of the wall shear rate in a plane (450 µm x 450 µm). At each measurement position, the complete time series of wall shear of a collapsing bubble (radius at maximum expansion: $R_{\max} \cong 425$ µm) is recorded. Thus, one bubble needs to be generated for each measurement position. The preferred means for the repeatable production of spherical cavitation bubbles of defined properties at a confined position is by the focusing of a laser pulse. In the laser focus, the power density is large enough to induce optical breakdown, i.e. a plasma is generated. Around the plasma, a cavitation bubble forms, a mechanism termed optical cavitation [11][12]. This mechanism is used here: a laser pulse (5 ns pulse duration, 532 nm, ~ 1 mJ) is focused close to the substrate (PMMA slide of 1 mm thickness) and the electrode (platinum electrode $d_E = 25$ µm diameter) into an aqueous solution in a glass cuvette of 125 ml volume. To avoid any spurious effects from the intense laser light, the laser beam is aligned vertical to the electrode surface (see [13]). With a high speed video camera, the bubble shape is imaged synchronized to the wall shear rate measurements allowing to relate the wall shear rate to the different stages of bubble dynamics. The wall shear rate is derived from a chronoamperometric measurement performed with a potentiostat of type Gamry Reference 600 that works at its maximum sampling frequency of 300 kHz. The sensor electrode is operated as working electrode, for counter and reference electrode a platinum wire is submerged close to the substrate. As buffer electrolyte KNO_3 is used. As analyte, a Faradaic electrolyte is dissolved in the deionized water ($Ru(NH_3)_6^{3+}$, concentration $c_0 = 0.03$ M). An electrical potential of $U_W = -0.7$ V is maintained between working electrode and counter electrode. It allows for the reversible reduction of the Ru-complex at the surface of the working electrode, in turn giving rise to a reduction current of:

$$I = \frac{FA_E \partial c(z,t)}{\partial z}\Big|_{z=0}, \qquad (1)$$

where F is the Faraday constant, A_E the electrode surface, c the concentration, and z the coordinate perpendicular to the electrode surface whereas $z = 0$ refers to the electrode surface [14]. The reaction kinetics of the Ru-complex are very fast, so a molecule of the Ru-complex can be considered to be reduced instantaneously, once it is found at the electrode surface. Therefore, the reaction current is limited only by the rate at which molecules of the Ru-complex reach the electrode. This rate is limited here only by diffusion and convection. The equation describing the concentration change is the convection diffusion equation. It reads:

$$\frac{\partial c(\vec{x},t)}{\partial t} = D\Delta c(\vec{x},t) - \vec{u}(\vec{x},t)\nabla c(\vec{x},t)\,, \qquad (2)$$

where D is the diffusion constant, c the concentration, and $\vec{u}$ the velocity. Here, by convection, the cavitation bubble increases the transfer rate of the electrolyte concentration to the electrode. This effect is exploited here. For the present situation, Equation (2) can be simplified: The electrode is operated as a macro electrode. This is achieved by the application of the working potential in sufficiently short intervals. Then, the flux to the electrode is planar, allowing for a one-dimensional treatment. Furthermore, the diffusion layer thickness δ is smaller than d_{E}. Within the small diffusion layer at the solid ($\delta < 25$ µm), the flow can be assumed to be parallel to the boundary and the flow profile is assumed to be linear. With these assumptions one arrives at the following parabolic differential equation for the wall shear rate $G(t) = \frac{\partial u(t)}{\partial z}\Big|_{z=0}$, where u is the x-component of the flow velocity:

$$\frac{\partial c(z,t)}{\partial t} = D\,\frac{\partial^2 c(z,t)}{\partial z^2} + G(t)\frac{z}{d_{\mathrm{E}}}\left(c_0 - c(z,t)\right). \quad (3)$$

In Equation (3), the wall shear rate appears as a source term. Its determination is an implicit problem. We solve it here with an optimization approach. For different candidates of G, the concentration profile was simulated using the toolbox Matlab (pdepe function). For each concentration profile, the resulting electrical currents were calculated. Then G was selected as the value at which the simulated current equals the measured current I. More details on this procedure and on the wall shear rate microscope can be found in [15]. From the wall shear rate, the wall shear stress s can be calculated by: $s = \mu G$, where μ is the viscosity of water.

Numerical methods

The bubble collapse is simulated using the density based CavitatingFoam solver of OpenFOAM. It is a fully compressible two-phase flow solver that applies barotropic equations of state and an Euler-Euler approach to solve the Navier-Stokes equations on a fixed Eulerian grid, considering gas and liquid phases as homogeneous mixture. Here, the liquid phase is water, the gas phase is water vapor. The mass fraction of the vapor in the mixture α is assumed to be a continuous function of space and time. It is determined as:

$$\alpha = \frac{\rho_{\mathrm{m}} - \rho_{\mathrm{w,sat}}}{\rho_{\mathrm{v,sat}} - \rho_{\mathrm{w,sat}}}, \quad (4)$$

where ρ_{m} is the mixture mass density, $\rho_{\mathrm{w,sat}}$ is the density of water at saturation and $\rho_{\mathrm{v,sat}}$ is vapor saturation density. Drop in the saturated liquid density below vapor saturation density indicates the presence of cavitation. $\alpha = 0$ means the presence of only the liquid phase, whereas $\alpha = 1$ indicates cavitation zones. The mixture compressibility φ_{m} is modelled using Wallis linear model [16] given by:

$$\varphi_{\mathrm{m}} = \alpha\varphi_{\mathrm{v}} + (1-\alpha)\varphi_{\mathrm{w}}, \quad (5)$$

where φ_{v} and φ_{w} are the liquid and the vapor compressibility. Further, the mixture viscosity μ_{m} is computed as:

$$\mu_{\mathrm{m}} = \alpha\mu_{\mathrm{v}} + (1-\alpha)\mu_{\mathrm{w}}, \quad (6)$$

where μ_{w} and μ_{v} are the viscosity of water and vapor respectively. The relation between pressure and density is defined as:

$$\frac{D\rho_{\mathrm{m}}}{Dt} = \varphi\,\frac{DP}{Dt}. \quad (7)$$

Above equation can be used directly in the continuity equation to formulate a pressure equation or integrated to obtain the pressure as a function of the density.

Simulations are carried out in a three dimensional domain without the assumptions of any symmetries in order to also simulate the bubble dynamics after the first collapse, when many bubble related phenomena become inherently three

dimensional. The size of the computational domain is 5 x 5 x 5 mm^3. Figure 1 (right) illustrates the plane section of the finite volume discretized domain. The flow is assumed to be laminar. The maximum acoustic Courant number is limited to 0.5 by choosing appropriate time steps. To reduce computational costs, the grid is refined to a minimum cell size of 6.25 µm only in region of interest, i.e. the collapse region. Furthermore, the bubble is initialized at its maximum expansion, defining the initial internal pressure and vapor volume fraction. Thus, the initial expansion from plasma seeding to maximum expansion is not simulated.

Results

An overview over the bubble dynamics is given in Figure 2 through the evolution of the bubble shape. The bubble collapses in vicinity to the substrate with the integrated wall shear rate sensor. The bubble was seeded at $t = 0$ µs. The bubble life time T_L is defined as the time from bubble generation (plasma seeding) to bubble collapse. Here, times are given in normalized form $\tau = t/T_\mathrm{L}$, where $T_\mathrm{L} \cong 89$ µs.

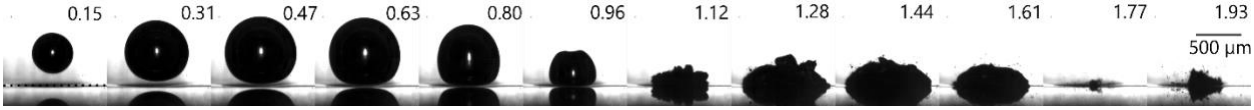

Figure 2 Photographic image series of the time evolution of the bubble shape. Normalized time τ are given in the top right corner of each image. The rigid boundary is depicted in the first frame. On the solid surface a mirrored image of the bubble shape is visible.

From $\tau = 0$ to $\tau = 0.5$ the bubble expands radially. After $\tau = 0.5$, the bubble collapses, initially in a merely spherical manner, towards the end of the collapse phase, increasingly aspherically. At $\tau = 0.96$, a small indentation on the bubble north pole is visible, a consequence of the jet that pierces the bubble and impacts perpendicular on the substrate [12]. After the collapse, at $\tau = 1.00$, the bubble is in the rebound phase up to $\tau \cong 1.35$: it takes a flat shape and spreads directly over the boundary. The bubble now has a toroidal shape [17][18], which is however not visible in this side projection. Then, the bubble collapses (toroidally) at $\tau \cong 1.75$. After the second collapse, main parts of the bubble have disintegrated and only a small bubble in the center shows some afterbounces.

In Figure 3 the respective shear rates are shown for four instances of time, in the top column experimental data is shown, in the bottom column data obtained from the numerical simulation. At the time instance $\tau = 0.72$, the bubble only undergoes a radial oscillation (sometimes called volume pulsation), i.e. it remains merely spherical. During this type of dynamics, wall shear rates are very low. Below the bubble center they are minimum because a stagnation area is formed. At the next time instance, $\tau = 1.03$, the jet has pierced the bubble and impacts on the substrate. From the jet impact, wall shear rates are now about 25 times larger. At the axis of symmetry, again a stagnation area, this time from the jet, is formed. At $\tau = 1.23$, the wall shear rates are still large as the bubble rebounds at the substrate. Thereby liquid is accelerated annularly outwards. The ring of high wall shear consequently expands radially (not shown here). The figure at $\tau = 1.73$ presents an intriguing situation. The (toroidal) bubble is about to collapse. Now, the highest wall shear rates are measured $G_\mathrm{max} = 5.88\ 10^6\ \mathrm{s}^{-1}$ during the situation in which flows directed inwards from the outer torus wall and the flows from the inner torus wall directed outwards collide.

After this collision of flows, no significant shear forces are anymore actuated on the solid surface. This is consequence of the formation of a ring vortex that is ejected from the surface. Thereby, the moving liquid is convected remote from the solid surface into the bulk. Figure 4 illustrates the flow field, obtained from the numerical simulation. This behavior was experimentally observed and quantitatively investigated before [18].

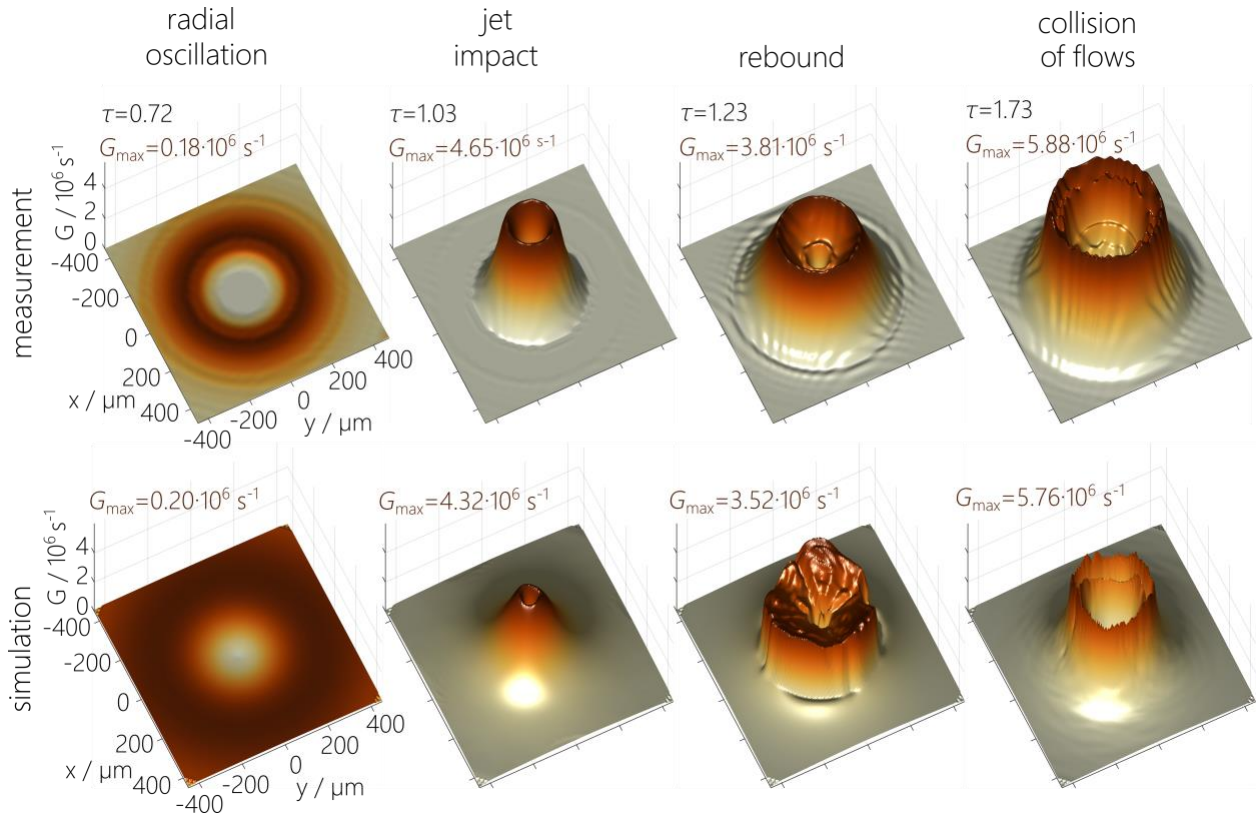

Figure 3 Comparison between measured wall shear rates (top column) and computed wall shear rates (bottom column) on the substrate surface. Four different times are chosen ($\tau = 0.72, \tau = 1.03, \tau = 1.23, \tau = 1.73$) that reflect different stages of the bubble dynamics (radial oscillation, jet impact, rebound, collision of flows). The data is height and color coded. The height coding is the same for every image (vertical axis wall shear rate $G = 0..6\ 10^6\ \mathrm{s}^{-1}$), the respective color levels are scaled to each maximum wall shear rate $G_{\max}$.

Both datasets shown in Figure 3 match well. They show the same features and almost the same maximum wall shear rates. This can be considered a confirmation for the numerical as well as the experimental method. However, differences between experiments and computations can be observed. In general, the experimental data shows a broadened structure, while according to the numerical computation, the wall shear rates seem to be locally more confined. A main reason for this appearance can be found in the experimental rastering methodology, in which the wall shear rates are measured from many bubbles. Even though we took measures to take into account only same-sized, spherical bubbles, still some jitter on the bubble life time (and consequently the geometric extension of the bubble at a given instance of time) is unavoidable. This jitter, is expected to geometrically smooth out the experimental data, and can be especially seen on the volcano-like structure that decays much smoother outwards in the experimental case (see $\tau = 1.72$). The accuracy of the numerical simulation could be increased by a finer spatial and temporal mesh size. Also, the spherical initialization of the bubble at its maximum expansion lets the simulated situation differ from the experimental one, where the bubble as it grows out of its plasma spot deforms due to the influence of the boundary. Also, the determination of the bubble stand-off distance to the wall is subject to some uncertainty. This is important because the stand-off distance is known to critically influence the bubble dynamics and consequently the generation of wall shear forces.

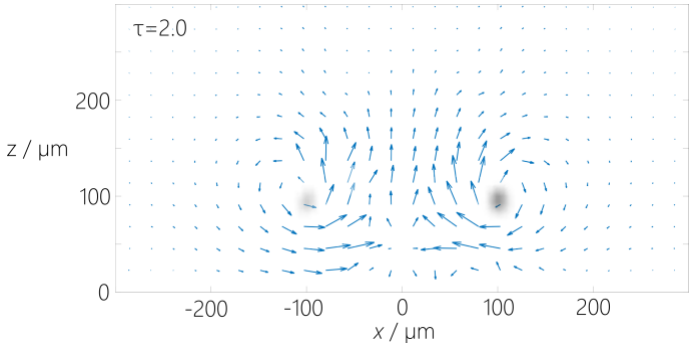

Figure 4 Flow field (simulated) after the detachment of the flow from the collision of flows has taken place and a ring vortex is formed, seen here in side projection. The boundary is located at $z = 0$. The gas phase is overlaid in gray.

Conclusion

A cavitation bubble generates intense microconvection directly at solid surfaces. A significant force transmission and potential surface alteration is induced by the wall shear flow. So far, experimental techniques for the measurement of the respective wall shear rate were limited. Here, the wall shear rates of a single collapsing cavitation bubble were measured in high spatial and temporal resolution. The wall shear rates were related to the bubble dynamics via synchronized high speed imaging. In addition, numerical simulations were carried out. The experimental results are consistent with numerical simulations. The wall shear rates during jet impact and toroidal bubble collapse could be quantified. They are shown to be the most significant ones generated by the bubble dynamics.

Acknowledgements

We thank Prof. Werner Lauterborn for constant commitment and scientific advice. F.R. and R.M. thank for the financial support by Lam Research AG, Austria, and by the Austrian Federal Ministry of Science, Research and Economy and the Austrian National Foundation for Research, Technology and Development.

References

[1] H. F. Okorn-Schmidt *et al.*, "Particle Cleaning Technologies to Meet Advanced Semiconductor Device Process Requirements," *ECS J. Solid State Sci. Technol.*, vol. 3, no. 1, pp. N3069–N3080, Dec. 2013.

[2] F. Reuter and R. Mettin, "Mechanisms of single bubble cleaning," *Ultrason. Sonochem.*, vol. 29, pp. 550–562, Mar. 2016.

[3] C. F. Naudé and A. T. Ellis, "On the Mechanism of Cavitation Damage by Nonhemispherical Cavities Collapsing in Contact With a Solid Boundary," *J. Basic Eng.*, vol. 83, no. 4, pp. 648–656, 1961.

[4] Y. Tomita and A. Shima, "Mechanisms of impulsive pressure generation and damage pit formation by bubble collapse," *J. Fluid Mech.*, vol. 169, pp. 535–564, Apr. 1986.

[5] W. Lauterborn and T. Kurz, "Physics of bubble oscillations," *Rep. Prog. Phys.*, vol. 73, no. 10, p. 106501, Oct. 2010.

[6] K. R. Rau, A. Guerra, A. Vogel, and V. Venugopalan, "Investigation of laser-induced cell lysis using time-resolved imaging," *Appl. Phys. Lett.*, vol. 84, no. 15, p. 2940, 2004.

[7] A. Vogel, P. Schweiger, A. Frieser, and M. N. Asiyo, "Intraocular Nd : YAG Laser Surgery : Light-Tissue Interaction , Damage Range , and Reduction of Collateral Effects," *IEEE J. Quantum Electron.*, vol. 26, no. 12, pp. 2240–2260, 1990.

[8] J. L. Compton, A. N. Hellman, and V. Venugopalan, "Hydrodynamic determinants of cell necrosis and molecular delivery produced by pulsed laser microbeam irradiation of adherent cells," *Biophys. J.*, vol. 105, no. 9, pp. 2221–2231, 2013.

[9] C. F. Delale, Ed., *Bubble Dynamics and Shock Waves*. Springer, 2013.

[10] "OpenFOAM 2.3.x, OpenFOAM Foundation, www.openfoam.org." 2015.

[11] W. Lauterborn, "Kavitation durch Laserlicht ('Cavitation by laser light')," *Acustica*, vol. 31, no. 2, pp. 51–78, 1974.

[12] W. Lauterborn and H. Bolle, "Experimental investigations of cavitation-bubble collapse in the neighbourhood of a solid

boundary," *J. Fluid Mech.*, vol. 72, no. 2, pp. 391–399, Nov. 1975.
[13] F. Reuter, C. Cairós, and R. Mettin, "Vortex dynamics of collapsing bubbles: Impact on the boundary layer measured by chronoamperometry," *Ultrason. Sonochem.*, vol. 33, pp. 170–181, Nov. 2016.
[14] J. Wang, *Analytical Electrochemistry*, Third edn. Wiley-VCH, 2006.
[15] F. Reuter and R. Mettin, "Electrochemical wall shear rate microscopy of collapsing bubbles," *Submitt. to Phys. Rev. Fluids*, 2017.
[16] G. B. Wallis, *One-dimensional two-phase flow*. New York, NY: McGraw-Hill Publishing Co., 1969.
[17] O. Lindau and W. Lauterborn, "Cinematographic observation of the collapse and rebound of a laser-produced cavitation bubble near a wall," *J. Fluid Mech.*, vol. 479, pp. 327–348, 2003.
[18] F. Reuter, S. R. Gonzalez-Avila, R. Mettin, and C.-D. Ohl, "Flow fields and vortex dynamics of bubbles collapsing near a solid boundary," *Phys. Rev. Fluids*, vol. 2, no. 6, p. 64202, Jun. 2017.